Thermal distribution characteristic of high-power laser double-cladding Thulium-doped fiber amplifier

Zhang Haiwei[1,2], Sheng Quan[1,2], Shi Wei[1,2], Bai Xiaolei[1,2], Fu Shijie[1,2], Yao Jianquan[1,2]

(1. College of Precision Instrument and Opto-electronics Engineering, Tianjin University, Tianjin 300072, China;
2. Key Laboratory of Opto-electronics Information Technology, Ministry of Education, Tianjin University, Tianjin 300072, China)

Abstract: The three-dimension thermal distributions in double-cladding high-power Thulium-doped fiber amplifier (TDFA) with different inner-cladding shapes were achieved by solving the analytical thermal conductive equation with different inner-cladding boundary conditions. It indicates that the temperature difference induced by the overlap factor of double-cladding fibers (DCFs) with different inner-cladding shapes can be up to 107 K in the core. Moreover, the distance between the splice point and the position with maximum temperature relies on the ratio of the seed power to pump power and it can be 30 cm when pumped with 100 W and seeded with 10 mW. By analyzing the transverse and longitudinal thermal distribution, it is demonstrated that the offset DCF may be a better choice for TDFA due to its lower maximum temperature, high pump efficiency and Gaussian thermal distribution on the cross-section.

Key words: Tm-doped fiber amplifiers; thermal effects; double-cladding fiber; analytical model
CLC number: TN248 **Document code:** A **DOI:** 10.3788/IRLA201746.0622004

高功率双包层掺铥光纤放大器温度分布特性

张海伟[1,2],盛 泉[1,2],史 伟[1,2],白晓磊[1,2],付士杰[1,2],姚建铨[1,2]

(1. 天津大学 精密仪器与光电子工程学院,天津 300072;
2. 天津大学 光电信息技术教育部重点实验室,天津 300072)

摘 要: 通过对普适于不同内包层边界条件下的热传导方程进行推导和求解,得到了不同内包层形状的双包层增益光纤所对应的掺铥光纤放大器的三维热分布。计算结果表明,双包层光纤不同内包层形状可导致纤芯处的温度差高达 107 K。同时,信号光与泵浦光功率的比值决定了温度最高点和熔接点的距离,在泵浦光功率为 100 W、信号光功率为 10 mW 的情况下,两者之间的距离可达 30 cm。通过分析不同内包层形状的双包层光纤的径向与轴向的热分布情况发现,相较于其他内包层形状的双包层光纤,偏芯型双包层掺铥光纤因其具有较低的最高温度、较高的泵浦效率和高斯型横截面热分布而较适用于掺铥光纤放大器。

关键词: 掺铥光纤放大器; 热效应; 双包层光纤; 解析模型

收稿日期: 2016-10-05; **修订日期:** 2016-11-03

基金项目: 国家高技术研究发展计划(2014AA041901);国家自然科学基金(61335013,61275102);
天津市科技支撑重点项目(2015ZDJS02001);山东自主创新与成果转化项目(2014ZZCX04212)

作者简介: 张海伟(1988-),男,博士生,主要从事光纤激光器和光纤传感方面的研究。Email:zhanghaiwei@tju.edu.cn

导师简介: 史伟(1964-),男,教授,博士生导师,主要从事光纤激光器、非线性光学和太赫兹方面的研究。Email:shiwei@tju.edu.cn

0 Introduction

High-power fiber lasers operating in 1 μm, 1.5 μm and 2 μm ranges have been achieved by employing all-fiber double-cladding pump technology via master-oscillation power-amplifier system[1-3]. Their advantages such as compactness, excellent beam quality, robust and high performance operation free maintenance, have made them be widely applied in nonlinear frequency conversion, surgery, industrial fabrication, defense and security, and so on[4]. High power thulium-doped fiber (TDF) lasers attract more attention among them for their large spectral range and high efficiency, characteristics of processing plastics, glasses and some biological and organic materials with water content as well as the high quantum efficiency, which can be up to 200% due to the energy cross-relaxation effect when using $^3H_6 \rightarrow {}^3H_4$ energy level pump scheme with 793 nm[5]. However, this pump scheme has a relatively higher quantum defect heating (>55%) in the Tm-doped fiber amplifier (TDFA), which makes it necessary to consider the heat generated in the amplifier, especially when it operates in high-power mode. Due to the propagation of helical fiber modes in circular DCF makes only a fraction of the pump light be absorbed, octagon, D-shape, rectangular and offset DCF have been proposed to improve the absorption efficiency[6]. It is necessary to analyze the thermal characteristic of DCF, considering that the different thermal distribution induced by the inner-shape of cladding may destroy the Gaussian profile of signal and the pump-induced heating may also degenerate the beam quality for thermal-induced refractive index changes[7-8].

In this paper, we establish the three-dimension thermal distribution model by employing thermal conductive equation and expressions of boundary conditions for different inner-cladding shapes. The transverse and longitudinal thermal distribution are achieved via solving the analytical three-dimension thermal distribution expressions considering mode-field radius in cylindrical coordinates. Then, we analyze the characteristic of maximum temperature and points with maximum temperature as a function of seed powers. It is shown in the results that the thermal difference induced by the inner-cladding shape of DCFs can be about 107 K under a pump power of 100 W. The ratio of the seed power to the pump power has an effect on the extraction efficiency of signal to upper-level populations and then influences the distance between the splice point and the position with maximum temperatures, which can be up to 30 cm. Moreover, it is demonstrated that increasing ratio of seed power to pump power can make the position with maximum temperature move to the splice point. Due to the lower maximum temperature, higher pump efficiency and Gaussian thermal distribution on the cross-section compared with others, the offset DCF is expected to be more suitable for TDFA.

1 Analytical thermal distribution

Figure 1(a) shows the schematic diagram of a high-

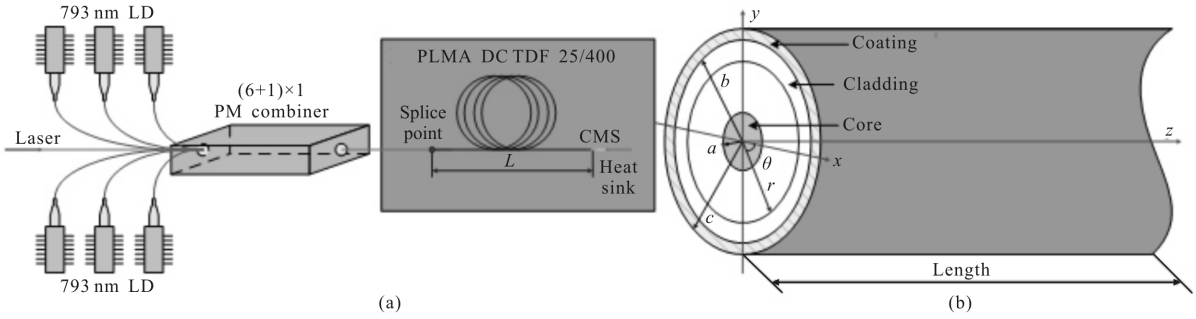

Fig.1 Schematic diagram of (a) forward-pumping TDFA and (b) DCF

power polarization-maintained (PM) TDFA with forward-pumping scheme, which consists of six 793 nm laser diodes, a $(6+1)\times1$ PM combiner, a cladding mode stripper(CMS) as well as a segment polarization-maintained large-mode-area (PLMA) double-cladding (DC) TDF with the length of L.

The structure of the DCF is illustrated in Fig.1(b). Considering that the inner and outer cladding have similar thermal conductivities, the DCF is assumed to be made up of the fiber core, the inner-cladding as well as the coating in order to simplify the process of solving the thermal conductive equation. Moreover, the coating a lower refractive index than the inner-cladding to satisfy the total-reflection condition for the light in the cladding. Because the capability of heat dissipation from the fiber side is much higher than the fiber end facet because of the large specific surface area, the three-dimension temperature distribution in the steady state can be expressed using the following thermal conductive equation in cylindrical coordinates [9-12]:

$$\frac{1}{r}\frac{\partial}{\partial r}\left(r\frac{\partial T(r,\theta,z)}{\partial r}\right)+\frac{1}{r^2}\frac{\partial^2 T(r,\theta,z)}{\partial \theta^2}+\frac{Q(r,\theta,z)}{K}=0 \quad (1)$$

Where, T, Q and K denote the temperature, heat density distribution in the fiber and thermal conductivity, respectively. r and θ are the radius and angle in cylindrical coordinates. The temperature changes along the angle θ in cylindrical coordinates can be neglected when the angle is divided small enough and the heat conduction is assumed to happen only along radius:

$$\frac{1}{r}\frac{\partial}{\partial r}\left(r\frac{\partial T(r,\theta,z)}{\partial r}\right)+\frac{Q(r,\theta,z)}{K}=0 \quad (2)$$

When the absorbed pump source converts into either laser signal or heat and the signal generated in the core of Tm-doped fiber has an almost Gaussian profile, the volumetric heat density has the following expression[12-13]:

$$Q(r,\theta,z)=\frac{Q_L(z)}{S}\cdot\left(\beta-\mathrm{e}^{\frac{-2R^2(r,\theta)}{\omega^2}}\right) \quad (3)$$

Where, $Q_L(z)=(1-\eta)\Delta P_p/\Delta z$, η is the conversion efficiency from absorbed pump to signal and ΔP_p is the absorbed pump power, which can be achieved by solving the rate equations for TDFA operating in the steady state[14]. S is the area of the fiber core. The normalized constant β and mode radius ω can be calculated by[13,15]:

$$\beta=1+\frac{\omega^2}{2a^2}\left(1-\mathrm{e}^{-\frac{2a^2}{\omega^2}}\right) \quad (4)$$

$$\omega=a\left(0.65+\frac{1.619}{V^{3/2}}+\frac{2.879}{V^6}\right) \quad (5)$$

It is assumed that the heat is only generated in the fiber core considering the pump light is mainly absorbed by the Tm^{3+} in the fiber core. Therefore, we can use the continuity of temperature at the boundaries among the fiber core, inner-cladding, coating and heat sink to get the thermal distribution expression as:

$$T(r,\theta,z)=\begin{cases}
T_0+\dfrac{Q_L(z)}{S\cdot K}\cdot\left[\dfrac{\beta-1}{4}R_{\mathrm{core}}^2(r,\theta)+\dfrac{1}{8\omega^2}R_{\mathrm{core}}^4(r,\theta)-\dfrac{\beta-1}{4}r^2-\dfrac{1}{8\omega^2}r^4\right]- & \\
\left[\dfrac{Q_L(z)}{S\cdot h\cdot c}+\dfrac{Q_L(z)}{S\cdot K_{\mathrm{ac}}}\cdot\ln\dfrac{R_{\mathrm{coating}}(r,\theta)}{R_{\mathrm{cladding}}(r,\theta)}+\dfrac{Q_L(z)}{S\cdot K}\cdot\ln\dfrac{R_{\mathrm{cladding}}(r,\theta)}{R_{\mathrm{core}}(r,\theta)}\right]\cdot & 0<r<R_{\mathrm{core}}(r,\theta)\\
\left[\dfrac{1-\beta}{2}R_{\mathrm{core}}^2(r,\theta)-\dfrac{1}{2\omega^2}R_{\mathrm{core}}^4(r,\theta)\right] & \\
T_0-\left[\dfrac{Q_L(z)}{S\cdot h\cdot c}+\dfrac{Q_L(z)}{S\cdot K_{\mathrm{ac}}}\cdot\ln\dfrac{R_{\mathrm{coating}}(r,\theta)}{R_{\mathrm{cladding}}(r,\theta)}+\dfrac{Q_L(z)}{S\cdot K}\cdot\ln\dfrac{R_{\mathrm{cladding}}(r,\theta)}{r}\right]\cdot & R_{\mathrm{core}}(r,\theta)<r<R_{\mathrm{coating}}(r,\theta)\\
\left[\dfrac{1-\beta}{2}R_{\mathrm{core}}^2(r,\theta)-\dfrac{1}{2\omega^2}R_{\mathrm{core}}^4(r,\theta)\right] & \\
T_0-\left[\dfrac{Q_L(z)}{S\cdot h\cdot c}+\dfrac{Q_L(z)}{S\cdot K_{\mathrm{ac}}}\cdot\ln\dfrac{R_{\mathrm{coating}}(r,\theta)}{r}\right]\cdot\left[\dfrac{1-\beta}{2}R_{\mathrm{core}}^2(r,\theta)-\dfrac{1}{2\omega^2}R_{\mathrm{core}}^4(r,\theta)\right] & R_{\mathrm{cladding}}(r,\theta)<r<R_{\mathrm{coating}}(r,\theta)
\end{cases} \quad (6)$$

Where, T_0 is the temperature of heat sink. h is the coefficient of surface heat transfer. K_{ac} is the thermal conductivity between the coating and the heat sink. $R_{\mathrm{core}}(r,\theta)$, $R_{\mathrm{cladding}}(r,\theta)$ and $<R_{\mathrm{coating}}(r,\theta)$ are the fiber core,

inner-cladding and coating boundary, respectively.

2 Boundary conditions and transverse thermal distribution characteristics

In order to improve the absorption efficiency and carry out high-power lasers, it is necessary to optimize the inner-cladding shape and parameter of DCF. As the cross-sections of different DCFs illustrated in Fig.2, the radial thermal distribution is confined by three boundaries: the fiber-core boundary $R_{\text{core}}(r,\theta)$, the inner-cladding boundary $R_{\text{cladding}}(r,\theta)$ and the coating boundary $R_{\text{coating}}(r,\theta)$. Considering most DCFs have a circular fiber core and coating, the inner-cladding boundary is the main factor that influences the thermal distribution. All the values for parameters used in the simulation are listed in Tab.1, in which Γ, σ, τ, α, and k are corresponding to overlap factor, cross-section, loss and cross relaxation rate, respectively.

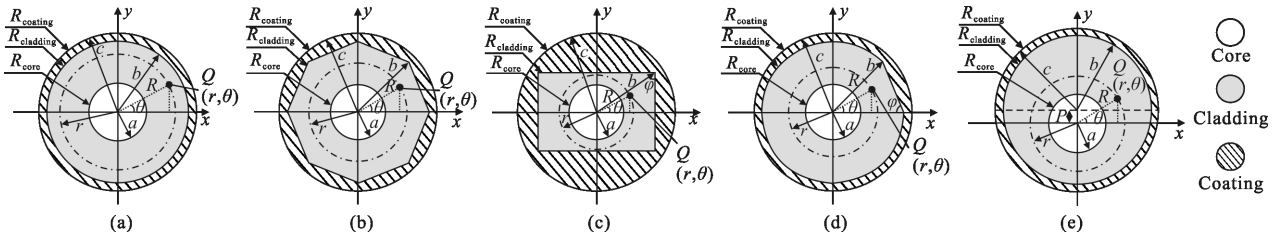

Fig.2 Cross-sections of (a) circular, (b) octagon, (c) rectangular, (d) D-shape, and (e) offset DCF

Tab.1 Parameters used in the simulation

Parameter	Value	Parameter	Value	Parameter	Value
λ_s/nm	1 925	r_{core}/μm	12.5	h/J·s	6.626×10^{-34}
λ_p/nm	793	r_{cladding}/μm	200	p/μm	50
λ_{ASE}/nm	1 600–2 100	r_{coating}/μm	275	Δz/m	1×10^{-3}
$\Delta\lambda$/nm	1.75	L/m	2	σ_{03}/m^2	8.5×10^{-25}[5]
τ_{31}/ms	0.337[5]	Γ_s	0.85	σ_{01}	[14]
τ_{10}/ms	0.014[5]	$\Gamma_{\text{p\_circular}}$	0.50×10^{-2}	σ_{10}	[14]
k_{3011} /m^3·s^{-1}	1.8×10^{-22}[5]	$\Gamma_{\text{p\_octagon}}$	1.11×10^{-2}	K /Wm^{-1}·K^{-1}	1.38[7]
k_{1130} /m^3·s^{-1}	1.5×10^{-23}[5]	$\Gamma_{\text{p\_d-shape}}$	1.03×10^{-2}	K_{ac} /Wm^{-1}·K^{-1}	0.2
$\alpha_{s-\text{loss}}$/m	5×10^{-3}	$\Gamma_{\text{p\_rectangular}}$	1.57×10^{-2}	T_0/K	298
$\alpha_{p-\text{loss}}$/m	5×10^{-3}	$\Gamma_{\text{p\_offset}}$	1.00×10^{-2}	–	–
N	2×10^{26}	c/m·s^{-1}	3×10^8	–	–

2.1 Circular and octagon double-cladding fibers

The model for solving the transverse thermal distribution of a circular DCF is shown in Fig. 2(a). The radii of fiber core, inner cladding and coating are assumed to be a, b and c, respectively. Considering a point $Q(r,\theta)$ on the cross-section of a circular DCF with different positions, therefore, we can obtain the cladding boundary equation in cylindrical coordinates easily:

$$R(r,\theta)=r,\ 0<\theta<2\pi \tag{7}$$

According to Eq. (6) and the inner-cladding boundary equation that $R_{\text{cladding}}(r,\theta)$ is equal to $R(b,\theta)$, we can get the radial temperature distribution of the circular DCF as depicted in Fig.3(a).

As the cross-section of octagon DCF shown in Fig.2 (b), R denotes the distance between point Q and the coordinate origin, possessing an angle θ with the x axis. The radii of the fiber core and the coating are still assumed to be a and c. If the circumcircle radius of the octagon is assumed to be b, R can be expressed as:

$$R(r,\theta)=\frac{r\cdot\tan(\varphi)}{\sin[\theta-n(\pi-2\varphi)]+\cos[\theta-n(\pi-2\varphi)]\tan(\varphi)} \tag{8}$$

Where, $(n-1)(\pi-2\varphi)<\theta<n(\pi-2\varphi)$, $n=0,1,2,\cdots,7$. φ denotes half of the interior angular of octagon. In addition, Eq.(8) is suitable for the hexagon DCF when n takes value from 0 to 5 and φ denotes half of the interior angular of hexagon. By substituting the inner-cladding boundary equation $R_{\text{cladding}}(r,\theta)$ with $R(b,\theta)$, we get the radial temperature distribution of the octagon and hexagon DCF as illustrated in Fig.3 (b) and (c), respectively.

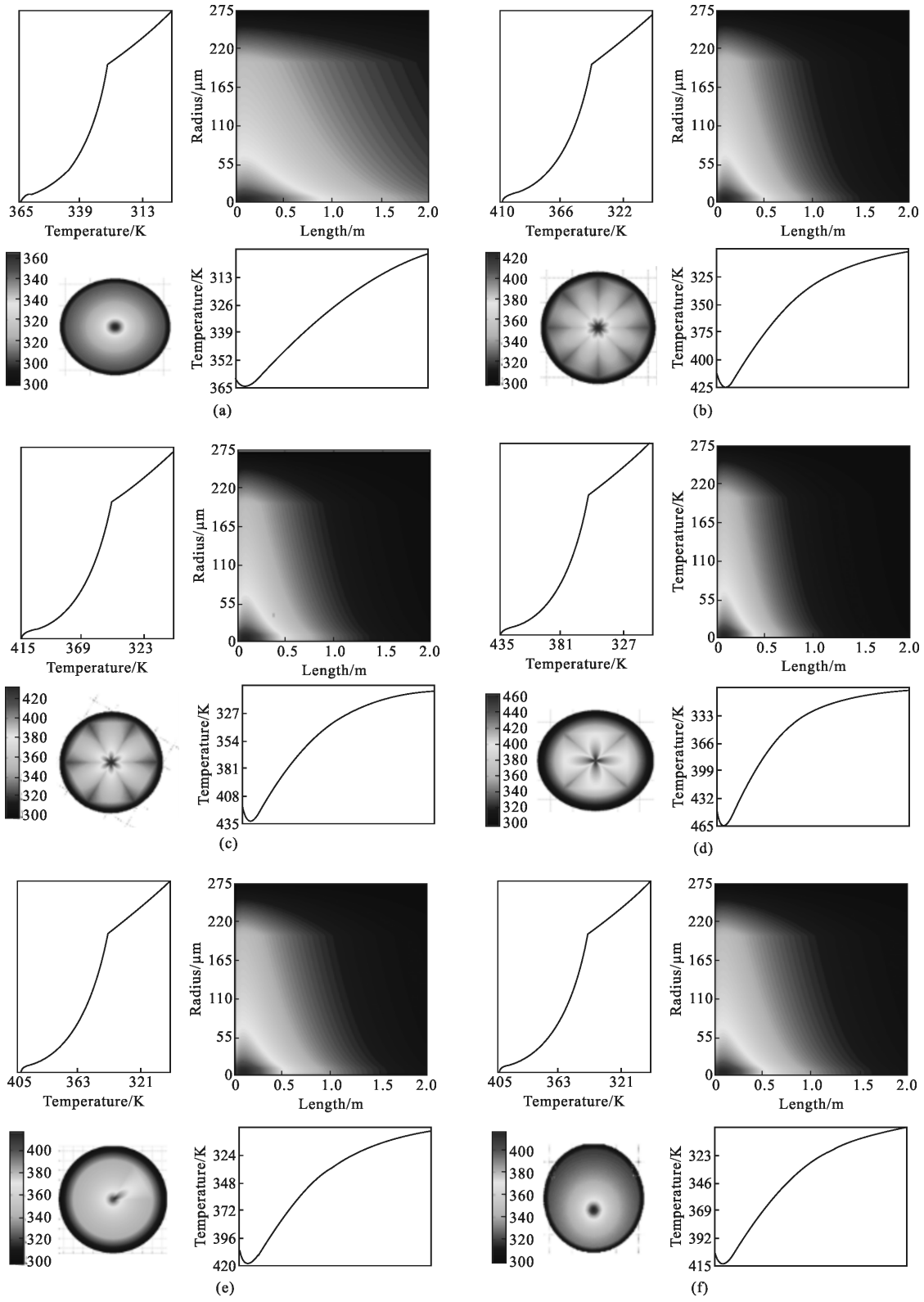

Fig.3 Transverse (circular) and longitudinal (square) temperature distribution of (a) circular, (b) octagon, (c) hexagon, (d) rectangular, (e) D-shape, and (f) offset DCF

2.2 Rectangular double-cladding fibers

As shown in Fig.2(c), the distance between point Q and the coordinate origin still defined as R, possessing an angle θ with the x axis. The circumcircle radius of

the rectangular is assumed to be b, therefore, R can be expressed as:

$$R(r,\theta)=\begin{cases}\dfrac{r\sin(\varphi)}{|\cos(\theta)|} & \dfrac{3\pi}{2}+\varphi+(n-1)\pi<\theta<\dfrac{5\pi}{2}-\varphi+(n-1)\pi,\ n=0,1\\ \dfrac{r\cos(\varphi)}{|\sin(\theta)|} & \dfrac{3\pi}{2}-\varphi+(n-1)\pi<\theta<\dfrac{3\pi}{2}+\varphi+(n-1)\pi,\ n=0,1\end{cases} \tag{9}$$

Where, φ denotes the angular between the radius and the edge perpendicular to the x axis. When $R_{\text{cladding}}(r,\theta)$ is equal to $R(b,\theta)$ in the thermal distribution expression, the calculated transverse thermal distribution of D-shape DCF is shown in Fig.3(d).

2.3 D-shape double-cladding fibers

Similar with the octagon DCF, R denotes the distance between point Q and the coordinate origin, possessing an angle θ with the x axis as shown in Fig.2(d). The distance R can be expressed as:

$$R(r,\theta)=\begin{cases}\dfrac{r\tan(\varphi)}{\sin(\theta)+\cos(\theta)\tan(\varphi)} & 0\leqslant\theta<\pi-2\varphi\\ r & \pi-2\varphi<\theta<2\pi\end{cases} \tag{10}$$

Where, φ denotes the angular between the straight edge of the inner cladding with the x axis. Therefore, the fiber-facet thermal distribution shown in Fig.3(e) can be calculated by using $R(b,\theta)$ to replace $R_{\text{cladding}}(r,\theta)$ in Eq.(6).

2.4 Offset double-cladding fibers

As it is depicted in Fig.2(e), an offset DCF with an offset distance p of the axis of the fiber core relative to the cladding and coating. R denotes the distance between the coordinate origin and point Q, possessing an angle θ with the x axis. Because of the offset distance p, the expressions of inner-cladding and coating boundaries in Eq.(6) are expressed as:

$$R_{\text{cladding}}(r,\theta)=p\sin(\theta)+\sqrt{b^2-p^2\cos^2(\theta)},\ 0<\theta<2\pi \tag{11}$$

$$R_{\text{coating}}(r,\theta)=p\sin(\theta)+\sqrt{c^2-p^2\cos^2(\theta)},\ 0<\theta<2\pi \tag{12}$$

Where, p denotes the offset distance relative to the axis of the fiber core. The calculated transverse thermal distribution of offset DCF is depicted in Fig.3(f). Moreover, we can find out in Fig.3 that the transverse thermal distribution of offset DCF has a Gaussian profile, which leads to a smaller degeneration of beam quality induced by thermal-induced refractive index changes compared with octagon, hexagon, D-shape and rectangular DCFs.

In order to protect the splice point between the passive and active fiber, we focus our attention on analyzing the maximum temperatures and the positions with maximum temperature versus seed powers by fixing pump power with 100 W as it is depicted in Fig.4. We can find out that the higher overlap factor makes the rectangular DCF has a higher maximum transverse temperature than the others. The maximum temperature difference induced by the inner-cladding shape of DCFs can be about 107K. It is also demonstrated that increasing the ratio of seed power to pump power makes the position with maximum temperature move to the splice point in the TDFA as the dash lines illustrated in Fig.4. And it indicates that there exists a ratio of seed power to pump power that has no influence on the positions with maximum power for all kinds of DCF.

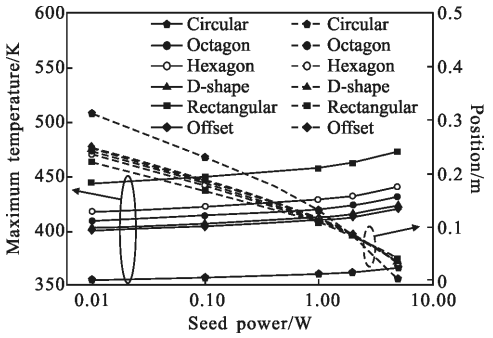

Fig.4 Seed powers versus maximum temperature (left) and positions with maximum temperature (right) for all kinds of DCFs

3 Longitudinal thermal distribution characteristics

Figure 5 illustrates the longitudinal temperature distribution of six types of DCFs as a function of fiber length with 100 W pump power and 2 W seed power. It is found that more pump power per unit

length is absorbed, generating more heat at the beginning of the DCF with a higher overlap factor. However, with the propagation of pump light in the active fiber, more pump power is residual for those DCFs with lower overlap factors, which leads to a higher temperature for its higher absorbed pump power per unit length at the end of the active fiber. As a result, rectangular DCF has the highest and the lowest temperature at the beginning and the end of the active fiber, respectively.

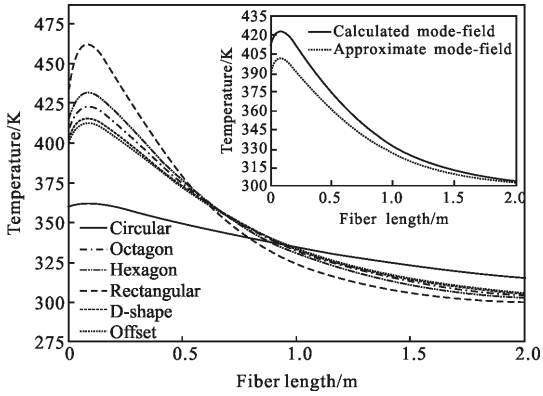

Fig.5 Longitudinal temperature distribution along different types of DCFs. Inset: the calculated temperature with (solid line) and without (dash line) mode-field approximate

In addition, the positions with maximum temperature do not locate in the splice point as it is depicted in Fig.5. It is considered that most of the populations are pumped into the upper-level $^3H_4$ due to the cross-relaxation effect and it is impossible for a small seed power to extract too much populations from the upper-level $^3F_4$ to the ground state $^3H_6$. As a result, the absorbed pump power is decreased for the ground-state depletion at the entrance to the active fiber. With the propagation of signal in the TDFA, the amplified signal leads to a higher extraction efficiency to the upper-level populations and increases the absorbed pump power in the unity of length, which raises the heat density and increases the temperature. It is consistent with the relationship between the seed power and positions with maximum power depicted in Fig.4. In order to investigate how the mode-field radius of the fiber core influences the thermal distribution in the DCF, we calculate and the longitudinal thermal distribution via the model in Ref. (11). As it is illustrated in the inset in Fig.5, approximating the mode-field radius using the fiber core makes a difference to the thermal distribution along the fiber core. It is indicated that the mode-area has no influence on the position with the maximum temperature, but effect the maximum temperature. And the maximum difference can be up to 20 K. Therefore, it is not suitable to substitute the radius of the mode with the fiber core when calculating the thermal distribution.

4 Conclusion

We propose the three-dimension analytical thermal distribution expression suitable for all kinds of DCFs and analyze their longitudinal and transverse thermal distributions by employing their analytical inner-cladding boundary conditions. Then, the maximum temperatures and positions with maximum temperatures of DCFs possessing different inner-cladding shapes as a function of seed powers are investigated. It is indicated that the maximum temperature difference induced by the overlap factor of inner-cladding can be 107 K. By influencing the extraction efficiency to the upper-level populations, the seed power has an effect on the distance between the splice point and the position with the maximum temperature, which can be 30 cm under a fixed pump power at 100 W. It is worth mentioning that 20 K temperature difference may be introduced by approximating the mode-field radius using the radius of fiber core in previous models. Considering the maximum temperature and Gaussian profile transvers thermal distribution, offset DCF is demonstrated to be a better choice for its high pump efficiency, low temperature and little destroy to the beam quality.

References:

[1] Wang W, Huang L, Leng J, et al. 2 kW CW near single mode all-fiber Ytterbium-doped fiber laser [J]. ***Optik***, 2015,

126: 1712−1715.

[2] Zhang X, Liu Y, He Y, et al. Characteristics of eye-safe high repetition frequency narrow pulse width single mode all fiber laser[J]. ***Infrared and Laser Engineering***, 2015, 44(4): 1105−1109. (in Chinese)

[3] Zhang H, Cao Y, Shi W, et al. Experimental investigation on spectral linewidth and relative intensity noise of high-power single-frequency polarization-maintained Thulium-doped fiber amplifier [J]. ***IEEE Photonics Journal***, 2016, 8 (3): 1−9.

[4] Shi W, Fang Q, Zhu X, et al. Fiber lasers and their applications [J]. ***Applied Optics***, 2014, 53(28): 6554−6568.

[5] Tao M, Huang Q, Yu T, et al. LD clad-pumped high efficient Tm−doped fiber lasers with different laser cavities [J]. ***Infrared and Laser Engineering***, 2013, 42 (8): 2008−2011.(in Chinese)

[6] Liu A, Ueda K. The absorption characteristics of circular, offset, and rectangular double-clad fibers [J]. ***Optics Communication***, 1996, 132(5): 511−518.

[7] Barmenkov Yu O, Kir′yanov A V, Andrés M V. Resonant and thermal changes of refractive index in a heavily doped erbium fiber pumped at wavelength 980 nm [J]. ***Applied Physics Letters***, 2004, 85(13): 2466−2468.

[8] Lu D, Ge T, Wu J, et al. Thermal stress induced birefringence in double cladding fiber with non-circular inner cladding [J]. ***Journal of Modern Optics***, 2009, 56(5): 638−645.

[9] Zenteno L. High-power double-clad fiber lasers [J]. ***Journal of Lightwave Technology***, 1993, 11(9): 1435−1446.

[10] Fan Y, He B, Zhou J, et al. Thermal effects in kilowatt all-fiber MOPA [J]. ***Optics Express***, 2011, 19 (16): 15162−15172.

[11] Xue D. Three-dimensional simulation of the temperature field in high-power double-clad fiber laser [J]. ***Optik***, 2011, 122 (10): 932−935.

[12] Rosa L, Coscelli E, Poli F, et al. Thermal modeling of gain completion in Yb−doped large-mode-area photonic-crystal fiber amplifier[J]. ***Optics Express***, 2015, 23(14): 18638−18644.

[13] Mohamme Z, Saghafifar H, Soltanolkotabi M. An approximate analytical model for temperature and power distribution in high-power Yb−doped double-clad fiber lasers [J]. ***Laser Physics***, 2014, 24(11): 115107.

[14] Fang Q, Shi W, Kieu K, et al. High power and high energy monolithic single frequency 2 μm nanosecond pulsed fiber laser by using large core Tm−doped germanate fibers: experiment and modeling [J]. ***Optics Express***, 2012, 20(15): 16410−16420.

[15] Marcuse D. Gaussian approximation of the fundamental modes of graded-index fibers [J]. ***Journal of the Optical Society of America***, 1978, 68(1): 103−109.